Title

A prototype Multi-X-ray-source array (MXA) for digital breast tomosynthesis

Journal

Physics in Medicine and Biology, 65(23)

ISSN

0031-9155

Authors

Becker, Amy E
Hernandez, Andrew M
Boone, John M
et al.

Publication Date

2020-12-07

DOI

10.1088/1361-6560/abc305

Peer reviewed

HHS Public Access

Author manuscript

Phys Med Biol. Author manuscript; available in PMC 2021 November 02.

Published in final edited form as:

Phys Med Biol. ; 65(23): 235033. doi:10.1088/1361-6560/abc305.

A prototype Multi-X-ray-source array (MXA) for digital breast tomosynthesis

Amy E Becker[1], **Andrew M Hernandez**[2], **John M Boone**[1,2], **Paul R Schwoebel**[3]

[1]Department of Biomedical Engineering, University of California Davis, Sacramento, CA 95817, United States of America

[2]Department of Radiology, University of California Davis, Sacramento, CA 95817, United States of America

[3]SRI International, Menlo Park, CA 94025 and Department of Physics, University of New Mexico, Albuquerque, NM 87131, United States of America

Abstract

The design and testing of a prototype Multi-X-ray-source Array (MXA) for digital breast tomosynthesis is reported. The MXA is comprised of an array of tungsten filament cathodes with focus cup grid-controlled modulation and a common rotating anode housed in a single vacuum envelope. Prototypes consisting of arrays of three-source elements and eleven-source-elements were fabricated and evaluated. The prototype sources demonstrated focal spot sizes of 0.3 mm at 45 kV with 50 mA. Measured x-ray spectra were consistent with the molybdenum anode employed, and the tube output (air kerma) was between 0.6 mGy/100 mAs at 20 kV and 17 mGy/100 mAs at 45 kV with a distance of 100 cm. HVL measurements ranged from 0.5 mm *Al* at 30 kV to 0.8 mm *Al* at 45 kV, and x-ray pulse widths were varied from 20 ms to 110 ms at operating frequencies ultimately to be limited by source turn-on/off times of ~1 ms. Initial results of reconstructed tomographic data are presented.

Keywords

digital breast tomosynthesis; stationary x-ray source; multisource x-ray

1. Introduction

The use of multiple x-ray sources in medical imaging systems that produce tomographic data is of interest for reasons ranging from reducing or eliminating mechanical motion to decreasing image acquisition times and system costs. The various approaches and their history have been thoroughly reviewed, (Neculaes *et al* 2014) so a summary is provided here which captures the key aspects as they relate to the technology underlying the Multi-X-ray-source Array (MXA).

paul.schwoebel@sri.com .

Beginning in the 1980's the earliest and most direct approach to incorporating multiple x-ray sources in imaging systems was implemented by the use of multiple conventional, rotating anode x-ray tubes, and such designs are commercially available today (Siemens SOMATOM Dual Source CT Scanners). About this same time sophisticated systems were developed in which an electron beam was scanned over a spatially distributed target to produce an x-ray source that moved through space without mechanical motion, creating a 'stationary' x-ray source (Boyd *et al* 1982). Subsequent approaches to multiple x-ray source systems grew to include the use of arrays of discrete, addressable cathodes distributed in space, often within a single vacuum envelope. These have been referred to as 'distributed x-ray sources' (Neculaes *et al* 2014). The cathodes used in distributed x-ray sources include thermionic cathodes (Kohl 1967) (tungsten filaments, dispenser, and oxide) and field electron emission cathodes (i.e. cold cathodes) (Zhu 2001). Such work continues to this day with arrays of cathodes being used to, for example, produce distributed x-ray sources for CT (Neculaes *et al* 2016, Kandlakunta *et al* 2017) and stationary x-ray sources for digital breast tomosynthesis (DBT) (Calliste *et al* 2017). For CT this source development has focused on the use of thermionic cathodes due to their proven performance and generally robust characteristics (Kohl 1967). Over the last decade the development of stationary sources for DBT has focused on the use of field electron emission cathode-based systems (Calliste *et al* 2017) due to attractive features (Neculaes *et al* 2014) such as their operation at room temperature. However in the case of field emission cathodes, unfortunately, despite efforts that started nearly 100 years ago (Kleint 1993) and subsequent support by large financial investments from both industry and government in the US and abroad, no commercially available medical imaging system using field emission cathodes is, or has been, used routinely in a clinical setting, principally due to their poor reliability in the x-ray tube environment (Sechopoulos 2013, Neculaes *et al* 2014).

To the best of our knowledge, all distributed x-ray source systems that have been reported in the scientific literature to date have employed stationary anodes (Neculaes *et al* 2014). X-ray tube anodes of course have inherent limitations to the sustained x-ray flux per source element they can support due to target heating considerations (Behling 2018, Oosterkamp 1948). In principle distributed x-ray source systems can employ enough individual source elements such that anode power densities per source element are acceptable for a stationary anode. However for tomographic imaging applications like DBT and CT, as the number of source elements is increased, the detector frame rate can become the rate-limiting step with respect to acquisition (scan) time. This can lead to systems with scan times that are too long to be clinically relevant (Neculaes *et al* 2014, 2016).

The other approach to increase the sustainable flux per source element is to use a rotating anode. Rotating anodes first became commercially available (Behling, 2018) in the late 1920's reflecting the need to increase the sustained output of bremsstrahlung x-ray tubes by distributing the electron beam power density over a larger anode surface area. A rotating anode can easily provide, for a given exposure time, ten-times the x-ray output of a stationary anode (Oosterkamp 1948). Although the use of rotating anodes in distributed x-ray source systems has been proposed generically (Neculaes *et al* 2014) and in the patent literature (Morgan 2000), there appears to be no published research in which a rotating anode-based distributed x-ray source has been investigated before 2019 (Boone *et al* 2019).

In this paper we discuss a prototype MXA system as a stationary x-ray source for DBT. The MXA employs tungsten filament-type cathodes for reliability, focus-cup grid control for modulation of the individual source elements, and a rotating anode to significantly increase the sustained x-ray flux per source element over that which can be achieved with a stationary anode. Besides the elimination of any possible image blurring effects due to x-ray tube movement or vibration inherent to a stationary source, (Tirada *et al* 2019, Horvat *et al* 2019) the associated simplified system design and reduction in system size has the potential to increase reliability and decrease capital, operating, and maintenance costs. In addition, the lack of mechanical motion associated with moving the x-ray source through space combined with the use of a rotating anode to increase the sustainable x-ray flux per source element imparts the potential to significantly reduce scan times relative to proposed (Calliste *et al* 2017) or existing (Tirada *et al* 2019) commercial systems. Scan time is one of the most important parameters of a DBT system (Smith 2013, Kopans 2014) with short scan times helping to minimize instances of image blurring due to patient motion.

2. Methods

2.1. Source design and fabrication

The MXA source uses an array of tungsten filament cathodes opposing a cylindrically symmetric, rotating anode. Grid-controlled cinefluoroscopy-type-tube cathode modulation is employed to define the beam spot (i.e. x-ray focal spot) size on the anode and allow for the individual x-ray source elements to be turned on and off. Figure 1 illustrates the rotating anode-based MXA source concept in DBT. Tungsten filament cathodes were chosen due to their simple, robust nature. For DBT, a stationary source replicating projection image positions of existing commercial systems requires: 1) Source densities of no greater than 1 source per degree of scan angle, equivalent to a linear power density of ~(24 W/filament) × (1 filament/2 cm) = 12 W cm^{-1} with a total power of 15 projections × (24 W/projection) = 360 W (Selenia Dimensions 3D; Hologic, Marlborough, MA, USA) and 2) and total power of less than 25 projections at 25 W = 600 W at a linear power density of ~(24 W/projection) × (1 filament/4 cm) = 8 W cm^{-1} (Mammomat with Tomosynthesis Option, Siemens Healthineers, Erlangen, Germany). These are manageable powers and power densities given typical x-ray source duty cycles.

For prototyping studies two 3-source element and one 11-source element MXA sources were designed, built, and tested. The 3-element sources (Boone *et al* 2019) served as a prototype for the 11-element DBT source. Figure 2 is a photograph of the first 3-element prototype and shows the molybdenum rotating anode opposing three focus-cup grid-controlled tungsten filament cathodes. In this version the rotating anode was machined from molybdenum rod-stock. Prototyping for a DBT MXA source will ultimately compare it with a commercially available system. For our initial studies we fabricated an 11-element anode with a source separation of 2.3 cm (equivalent to a total scan angle of 20°) to produce a projection number and scan angle between that of the Hologic Selenia Dimensions 3D (15 projections over 15°) and the GE Senoclair (GE Healthcare, Chicago, Illinois, USA) system (nine projections over 25°).

Although the machined-anode approach is physically robust and simple, it becomes costly and more difficult to fabricate as the diameter of the anode is increased for greater power handling capability and/or the number of source elements is increased. This is because in this approach, the amount of metal that is removed by the lathe is excessive. We have therefore transitioned to a modular approach in which anode components are fabricated and then brazed together.

The anodes were mounted on Varian RAD-92 x-ray tube rotor assemblies and driven by the associated Varian stator. For the 3-element prototype, a single RAD-92 bearing assembly was used. For the 11-source element MXA, two bearing assemblies were used with one at each end of the anode. Anode rotational speeds have been as high as 3600 rpm. For studies here anode speeds were maintained at 1000 rpm to limit bearing wear and because the combination of current (limited to 50 mA at 45 kV by the generator, a Spellman STR120P6 high voltage supply) and focal spot size (~0.3 mm × 1.0 mm) allowed these lower speeds. A photograph of the 11-source element MXA mounted on a demountable vacuum flange is shown in figure 3.

The source elements are focus-cup grid-controlled with a focus cup (grid) bias of one to several hundred volts negative with respect to the grounded filament used to form the line focus on the anode. A grid bias of between −1000 V and −1200 V is used to turn off the x-ray source elements. The source elements are operated using an in-house, custom-built source controller which controls the beam current on the anode, the beam focusing and turn-off voltages of the grid, the exposure time of each source, and the time between turning on and off each source element. The filament current of each individual source element is controlled allowing for the resulting tube current from the individual elements to be adjusted/tuned, e.g. to be the same. In these prototyping experiments positive HV was applied to the anode to allow the filament and grid control circuity to be at ground potential.

Source studies were conducted using an ion-pumped stainless-steel vacuum envelope to house the MXA source, see figure 4. This chamber was operated in the 10^{-7} to 10^{-6} Torr range during experiments. Electrical feedthroughs supply the filament power and focus-cup voltages. A custom built, 1-mm-thick rectangular aluminum x-ray window with dimensions of 35.0 cm × 3.8 cm forms a vacuum seal at the bottom of the envelope. The current field of view at a source to imager distance (SID) of 65 cm is 21 cm × 30 cm, sufficient to accommodate our upgrade to a Varian 2520 detector in the future. No fundamental source constraints prevent having field of views of 24 cm by 29 cm in order to be compatible with standard mammography/DBT detectors. Two commercial Conflat glass viewports were used to view the source assembly with a video camera during operation. No collimation was used for our prototyping experiments because the source was operated in an unoccupied room. Ultimately the MXA collimator would nominally consist of a metal (such as lead or tungsten) plate having perforations that appear as parallelograms when viewed in cross-section from the edge of the plate. The orientation of the perforations can be designed so as to keep the x-ray coverage slightly smaller than the active area of the detector and constant for each projection to help minimize the risk of irradiating non-breast portions of the patient. This can be done in a relatively straightforward manner using, for example, water jet machining.

2.2. Source evaluation

Fundamental operating parameters of the MXA source investigated were the x-ray spectrum, x-ray focal spot size, tube output, half value layer (HVL), and source modulation characteristics. X-ray spectra were measured using an Amptek XR-100 detector calibrated with ^{55}Fe and ^{241}Am x-ray standards. An anode angle of 12° was used throughout. Focal spot sizes were imaged with a 10 μm diameter pinhole (Nuclear Associates, Inc. Carle Place, NY, USA). Average spot sizes were measured using a star x-ray test pattern (Model 07–503, Nuclear Associates, Inc. Carle Place, NY, USA) which contains 60 spoke pairs divided into four 15° sectors wherein each spoke diverges at an angle of 0.5°). The tube output and HVL measurements were made using a dedicated mammography ionization chamber (10X5-6 M-3, RadCal Corp., Monrovia, CA, USA) connected to a model 9060 electrometer and a model 9010 readout unit (RadCal Corp., Monrovia, CA, USA). X-ray pulse shape versus time measurements were taken using an Amperex XP2262B photomultiplier tube and plastic scintillator with the output viewed by a Tektronix TDS540D oscilloscope.

Initial imaging characteristics of the prototype source were evaluated using a Varian PAXSCAN 1313 flat-panel x-ray detector based on an indirect thin-film transistor design and a CsI scintillator. The 1313 panel incorporates 127 μm pixels over a 13 cm × 13 cm field of view. The array of 1024 × 1024 pixels can be read out at up to 30 frames per second. The electronics associated with the flat-panel detector provides a 5 V transistor-to-transistor logic (TTL) pulse for each frame and this TTL pulse was integrated with the source controller to synchronize the firing of each x-ray source element. The source-to-detector distance was 72.5 cm. We are presently transitioning to the use of a Varian 2520 detector, see figure 4, which simply replaces the position of the Varian 1313.

Tomographic data sets and x-ray modulation experiments reported here were made with the 3-element MXA source serving as a prototype for the 11-element source. This is because the 11-source element controller, for which the 3-source element controller served as a prototype, is still under construction. In order to mimic the tomographic data set produced by an 11-element source, the detector was physically translated under the MXA source (3 element source position 1 served as 11-element source positions 1, 4, 7 and 10; 3 element source position 2 served as 11-element source positions 2, 5, 8 and 11; 3 element source position 3 served as 11-element source positions 3, 6 and 9. The phantom used for geometrical calibration was fabricated by cementing 1/16’ (1.59 mm) diameter stainless-steel spheres onto a 1/32’-thick (7.9 mm) sheet of Polymethylmethacrylate sheet (i.e. Lucite™) to form a regular right pyramid with one sphere at the apex and one at each of the four corners of the base. The base side-length of the pyramid was 1 cm and the height of the center of the sphere at the apex above the center of the spheres at the base was 8 mm.

3. Results

3.1. X-ray spectra

Figure 5 shows the x-ray spectrum from a single source element using electron beam energies ranging from 25 to 45 keV (in 5 keV intervals). The higher energies are typical for those required in DBT. The *K*-shell fluorescence lines of molybdenum at 19.6 keV and

17.4–17.5 keV are evident as peaks in the spectrum. As would be expected, no discernable difference was observed between the spectra produced by each of the 11-source elements given that the same electron energy, anode angle, and x-ray beam filtration was used for each element.

3.2. X-ray focal spots

Figure 6 shows x-ray pinhole camera images of a typical x-ray focal spot from a single source element as a function of voltage, V_{grid}, applied to the focus cup grid relative to the grounded filament. In the radiograph the anode is toward the 9 o'clock position and the filament/focus cup is toward the 3 o'clock position. As V_{grid} is decreased from 0 V there is a gradual decrease in the size of the focal spot perpendicular to its elongated direction. Optimal focusing was achieved with a V_{grid} between −200 V and −300 V for anode voltages between 35 kV and 45 kV. Here, about 80% of the x-rays emanate from within 0.3 mm of the spot centerline. As V_{grid} is decreased further, the spot becomes over focused and begins to broaden while there is a slight decrease in the width of the focal spot in the elongated direction as is evident in figure 6 at −400 V. A V_{grid} of −1200 V reduced the anode current to zero amperes. The pinhole images were taken with the pinhole located on the filament-side of the vertical line connecting the x-ray focal spot with the detector surface so as to view the focal spot without excessive geometrical foreshortening by the line focus principle.

An x-ray star pattern radiograph, taken with the same source element used to produce the pin-hole camera images in figure 6, is shown in figure 7. For spatial reference the anode is toward the 9 o'clock position and the filament/focus cup toward the 3 o'clock position. The star pattern was centered in the x-ray beam striking the detector, and the average focal spot size was determined to be 0.30 mm. In this position, the focal spot appeared to have nearly equal dimensions from each of the 11-source elements and varied by less than ~ ±10%.

3.3. X-ray tube output

The tube output was measured as a function of electron beam energy from 20 keV to 45 keV (in 5 keV intervals) as shown in figure 8 for a single source element. Because the filament current of each source element can be independently controlled, adjustments can be made to reduce the variation in output between source elements to ~5% or less (as measured directly below the source element).

3.4. Half-value layer

The HVL was measured at 50 mA between beam energies of 30 keV and 45 keV as shown in figure 9. These values for a molybdenum anode are reasonable given the 1-mm of aluminum filtration.

3.5. X-ray modulation

The focus-cup grid control was designed to be compatible with DBT systems using from 9 to 25 projections because these represent the range of most existing major manufacturer's systems (Tirada *et al* 2019). For example, take 100 mAs as a nominal total exposure for DBT, assume an operating current of 100 mA/source element, and use of an appropriate

DBT detector (such as the Varex Dexela CMOS 2923, which has 0.075-mm native detector elements and operates at 26 fps in the 1 × 1 binning mode). With these assumptions the maximum on-time for a given source element is (100 mAs/[100 mA/source]/9 sources) = 111 ms, at a source element switching frequency of (111 ms + 1/26 fps) = 149 ms/projection equivalent to ~7 Hz. The minimum on-time per source element and maximum operating frequency would occur with the source elements operating at the estimated (Oosterkamp 1948) 200 mA maximum of our system with 25 projections. In this case the individual source element on-time is (100 mAs/[200 mA/source]/25 sources) = 20 ms giving a source switching time of (20 ms + 1/26 fps) = 59 ms/projection equivalent to a rate of 17 Hz.

Figures 10 and 11 show, respectively, sequential x-ray pulses for each of the three individual elements comprising the 3-element MXA source in the low and high-speed switching cases above using currents of 40 mA at 35 kV. Figure 10(a) shows the TTL logic pulse used to control the focus cup grid potential and switch it from −1200 V (x-ray off) to −200 V (x-ray on at minimum focal spot). When the TTL signal is high the source is on. Figure 10(b) shows the x-ray output versus time with 110 ms wide x-ray pulses sequentially from each of the three MXA source elements at 7 Hz. Similarly figure 11 shows the x-ray output versus time with 20 ms wide x-ray pulses sequentially from each of the three elements at 17 Hz. Figures 10 and 11 demonstrate that the time required to modulate the x-ray output from each source element can address any of the range of possibilities required for existing DBT system designs. Note that because the output of each source element can be adjusted independently of the others by setting different filament currents, small variations in x-ray output between source elements can be achieved, as shown in figures 10 and 11.

3.6. Tomosynthesis data

Figures 12 and 13 are examples of tomosynthesis images reconstructed from data taken using the MXA. The orientation of the images is such that the right-hand side of the image is the anode-side of the MXA source. The total exposure was 100 mAs (9.1 mAs/element operating at 45 kV and 50 mA/element) in both cases. Figure 12 shows tomosynthesis images of the BB-calibration phantom at three depths with the planes separated by 4.0 mm. Figure 12(a) shows the plane in which the BB at the apex of the pyramidal phantom is in focus; figure 12(b), the plane half-way between the BB at the apex and the four BBs at the base of the pyramid; and figure 12(c) the plane in which the four BBs at the base of the pyramid are in focus. Figure 13 shows tomosynthesis images of an orange at three depths with the planes separated by 4.0 mm through the central core. The projections were reconstructed using simple shift and add for the BBs and matrix-inversion tomosynthesis for the orange. These are some of the first attempts at reconstructing tomographic data sets generated from projections acquired with the MXA.

4. Discussion

4.1. X-ray spectra

Figure 5 shows standard bremsstrahlung spectra from a molybdenum anode. Monte Carlo simulations and analytical modelling (Shrestha *et al* 2017) have indicated that roughly 1 mm of aluminum, as used in these studies, provides good filtration for DBT when tungsten

anodes are used. Longer term plans for this technology include cladding the molybdenum focal tracks with a tungsten/rhenium alloy, commonly employed outside of breast imaging applications for general purpose radiography and computed tomography. Tungsten anodes are also being used more frequently for breast imaging, with appropriate beam-softening filters such as rhodium, palladium and silver.

4.2. X-ray focal spots

Focal spot behavior with focus cup voltage is consistent between different source elements and spot sizes are consistent with those used in DBT. Note that the spot intensity distribution is not bimodal and this result is to be expected when using biased (as opposed to nonbiased) focus cups (Bushberg *et al* 2012). There are a number of geometrical variables that impact the focusing voltage required to optimize the spot size and turn-off the source element including the position of the filament within the focal cup, the dimension and shape of the cup, and the proximity and potential applied to the anode. Modeling is currently being used to further optimize the trade-offs involved.

4.3. X-ray tube output

The increasing x-ray production efficiency at higher voltages is evidenced by the increase in slope of the curve with increasing voltage (figure 8). The output of the MXA is comparable to that of clinical DBT systems. Our present operating current of 50 mA/source yields an air kerma rate of 5 mGy s^{-1} at 28 kV with the typical SID for mammography/DBT of 65 cm.

4.4. Half-value layer

The beam quality reported here meets the requirements set by the MQSA and the ACR for the range of half-value layers that are applicable for mammography with a *Mo* target and *Rh* filter combination. The effective x-ray energies referenced to the measured half-value layers are roughly, 18 keV (0.5 mm *Al*), 19 keV (0.6 mm *Al*), 20 keV (0.7 mm *Al*), and 21 keV (0.8 mm *Al*).

4.5. X-ray modulation

Key to the operation of the MXA source is modulation of the x-ray output from each individual source element with the focus cup grid voltage, that is with *grid control*. The modulation rate is linked to the scan time, i.e. the time required to generate the entire tomographic data set. As would be expected, x-ray element modulation times using grid-control techniques can be in the millisecond range and source on-time and modulation rates demonstrated here are easily high enough to handle current levels of 200 mA/source element. Scan time is in part dictated by the x-ray tube current and the application. The Hologic DBT system has the shortest scan time of commercial systems at 3.7 s for 15 projections (~70 mAs total exposure). Field electron emission-based stationary sources using stationary anodes have a scan time of ~3.1 s. (Calliste *et al* 2017) Currently, the MXA even operating at the demonstrated 50 mA/source element, has a scan time for 15 projections of (15 projections/26 fps + 70 mAs/50 mA) = 2.0 s, where we have assumed use of an appropriate DBT detector such as the Varex Dexela CMOS 2923 which has 0.075-mm native detector elements and operates at 26 fps in the 1 × 1 binning mode. The potential of the

MXA to further reduce scan time is significant. At 100 mA/source element the MXA scan time would be 1.3 s. If 200 mA/source element can be demonstrated, the scan time for 15 projections would by reduced to 0.9 s—at which point the detector frame rate is becoming a very significant rate limiting step with respect to total acquisition time.

4.6. Tomosynthesis data

The first studies of reconstructing tomographic data sets from the MXA source focused on using filtered backprojection (FBP) and matrix inversion tomosynthesis (MITS). The results of these initial studies are only preliminary, but it appears that MITS was more accurate than FBP, in that the intensity was more uniform within the slice, with the central slices. As our studies proceed, we plan with FBP, in addition to the standard ramp filter, to use a cosine-shaped anodization filter to suppress high-frequency noise. In addition, low frequency enhancement (Godfrey *et al* 2003, Mertelmeier 2014) will be used to restore some of the contrast suppressed by the ramp filter, so the images have less of a 'flat' appearance. With MITS, the sliding average approach that sums adjacent planes (Godfrey *et al* 2013) will be optimized for the number of slices to slab according to the response of microcalcifications with the given tube angle used. This sliding average technique reduces image noise while also suppressing most tomosynthesis artifacts. For FBP, a slabbing method will be used to best depict the three-dimensional spread of microcalcification clusters.

4.7. Source operation and design

4.7.1. Source-element performance consistency—Despite the fact that the MXA is only in the initial prototyping stage it is worthwhile to discuss aspects related to the consistency of performance between source elements. To date reasonable consistency between source elements in terms of x-ray spectrum, x-ray focal spot size, x-ray output, and tube (anode) current has been observed as presented in section 3. One aspect of the MXA that allows for matching the performance between individual source elements is that the filament current through each element can be controlled independently. This means that the tube current produced by each source element can be adjusted so as to balance the x-ray output and achieve highly similar outputs as shown in figures 10 and 11. In addition, the output of each source element can be varied to keep the x-ray fluence rate at the detector constant as the detector-to-source element distance changes due to the prototype's linear source-element geometry. X-ray focal spot sizes can be made very similar to one another across the array of 11-source elements (section 3.2), mainly by adequate control of geometrical variables just as is done for conventional commercial tubes of the same model. In addition, the grid-control feature of the MXA allows, in principle, for the use of different focus voltages for each source element to adjust to the focal spot size.

Given that the MXA is still in the prototyping stage long-term source stability studies are a future task. However, qualitatively, we have observed during the course of hundreds of experiments which involved cycling through source elements over weeks of operation, that filament current–voltage characteristics and the resulting tube currents are reproducible, and x-ray output per source element is consistent. In principle this is not surprising. The MXA design is the result of the integration of proven tube components to make, in essence, an array of conventional tungsten-filament-based, grid controlled, rotating-anode x-ray sources

operating in parallel within a common vacuum envelope. From this top level view one would then expect that the key characteristics such as the inherent lifetime and stability associated with filament performance, the reproducibility of source element output, and spot size variations between elements to be similar to those achieved with and between conventional rotating anode x-ray tubes of the same model, e.g. according to International Electrotechnical Commission standards.

4.7.2. Anode considerations—For initial prototyping, molybdenum anodes were used because molybdenum can be machined into various shapes by conventional methods, and because the power loading capability of molybdenum was adequate for initial testing. The x-ray tube current was limited to 50 mA by the x-ray generator. A transition to tungsten/rhenium cladding on the focal tracks on the anode is planned because it would not only provide an x-ray energy distribution that is better matched to DBT and CT imaging applications, but also would increase the allowable x-ray flux and power loading (W/cm^2) levels compared to molybdenum due to its higher Z and higher melting point.

The geometry of the MXA anode allows for effective cooling. First, the large surface-area-to-volume ratio of the MXA anode disk array increases its efficiency in radiating power relative to a standard rotating anode: The MXA anode shown in figure 3 has roughly twice the effective radiating surface area as a conventional 4’ diameter rotating anode and the radiated power is proportional to the radiating area. Secondly, liquid-cooling of the anode can be implemented by flowing the liquid (e.g. water) along the axis of the anode, i.e. in one end and out the other, possibly employing ferrofluid seals for the vacuum-to-atmosphere anode seal and water supply-to-anode seal. Roughly speaking it is practical to dissipate over 10 kW with water flow through a hollow-cylinder-based version of the anode shown in figure 3 (Reference Data for Radio Engineers 1981) whereas typical values of power dissipation by conduction through the ball bearings of a conventional tube are of order a few watts.

The brazing-based modular approach to fabricating the anode enables the design of more advanced anode configurations, such as stacked disks having diameters that gradually increase from the center of the field of view outward—with the anode faces machined at a fixed angle relative to the axis of rotation. This would mechanically steer the focal spot toward a common isocenter with the result that all of the focal spots would be located on a radius of curvature centered on the isocenter of the tomosynthesis system. Such a design would keep a constant x-ray focal spot size and source-to-isocenter distance by emulating the path of a single x-ray tube traveling through an arc. In addition, this design would still only need a simple, cylindrically symmetric vacuum envelope enclosure around the MXA source assembly. Implementation would require that the focal spots be spatially located on a compound curve, and this fabrication strategy is straightforward. A curved source array would allow use of existing tomosynthesis reconstruction algorithms, and balancing focal spot shape and size across all sources would reduce potential image artifacts.

4.7.3. Line focus and in situ variable anode angle—The line focus geometry used here has its elongated portion positioned in the direction of anode rotation, in contrast to the standard anode design in conventional tubes where the long axis of the focal track is normal

to the direction of anode rotation. For a given anode rotational speed and incident electron beam power density, this decreases the power loading (Oosterkamp 1948) by a factor of ~4 (the filament has a length of 5 mm which is roughly the beam spot length on the anode, and the width of the beam on the anode was measured to be 0.3 mm, so $[5\text{ mm}/0.3\text{ mm}]^{1/2}$ ~4). This design was a more straightforward geometry to employ for our prototyping studies. Estimates indicate, however, that a 5 cm diameter anode at 1000 rpm and an anode angle of 12° with 11 source elements can accommodate exposures of 100 mAs at 40 kV with 100 mA/(source element). Furthermore, we note that the existing geometry allows the anode angle to be varied *in situ* by deflecting the electron beam from each source element in the direction perpendicular to rotational axis of the anode. This deflection could be implemented using, for example, a second grid electrode placed between the focusing cup and the anode. In the existing assembly, this means that the anode angle could be varied from a few degrees to several 10's of degrees. Of course, changing the anode angle has a significant influence on the effective size of the focal spot, the x-ray fluence rate, the heel effect, and the field coverage of the beam at the detector.

The ability to change the effective focal spot size over a wide continuous range of dimensions has a number of usable applications in breast imaging and beyond. Decreasing the anode angle results in both a smaller x-ray focal spot and a smaller usable field of view. For magnification mammography and tomosynthesis applications, the anode angle could be dynamically adjusted to accommodate the variable field of view used in magnification imaging, allowing the smallest effective focal spot to be used for each field-of-view setting. Given the speed of acquisition capable with the MXA, each source element could actually produce two redundant images for each tomographic projection—one with a large focal spot and one with a smaller focal spot. This would result in one acquisition being high-pass and the other medium-pass filtered. With the appropriate use of image processing software (such as subtraction or deep learning versions of subtraction), harmonized (e.g. blurred-mask subtraction) projection images could be used to produced edge-enhanced (using physics, not just image processing) tomosynthesis reconstruction.

5. Conclusions

The proof-of-principle experiments were performed and clearly demonstrate the feasibility of the MXA source technology, comprised of an array of grid-controlled tungsten filaments and a rotating anode. The first prototype demonstrated operating characteristics consistent with x-ray tubes required for stationary source DBT. The functional MXA system was demonstrated, and tomosynthesis images were produced—demonstrating the first application of a tomosynthesis system employing a stationary x-ray source comprised of thermionic cathodes and a monolithic rotating anode. Even at this early stage the MXA has shown the potential to significantly reduce scan times relative to existing and proposed commercial systems.

Future goals are to increase the rotational speed of the anode to 3600 rpm and beyond while extending the tube current to 200 mA per source. Plans are in place to purchase a new generator providing 200 mA at 50 kV. Also a larger field-of-view flat panel detector (Varian 2520 with 0.127 mm detector element dimensions (Salt Lake City, UT)) is currently being

integrated into a compact tomosynthesis system for further imaging experiments. Lastly, we plan to integrate a MXA tube into a CBCT system on the rotating gantry, to reduce cone beam artifacts for applications including dental, orthopedic, breast, and image guided radiotherapy applications. Additional background and discussion of the potential benefits for applying the MXA source to CBCT is discussed in another publication (Becker *et al* 2020).

Acknowledgments

The authors gratefully acknowledge invaluable advice on rotating anode technology provided by Dennis Runnoe, Retired VP of Research and Development at Varian Medical Systems, Salt Lake City, UT. Professor James T Dobbins of Duke University is acknowledged for his tomographic reconstructions of the data and J A Seibert for pointing out the variable anode angle capabilities. Lastly, our work was greatly facilitated by commercial rotating anode assemblies provided by Robert Hibdon of Ray-Pac in N. Charleston, SC.

This research was supported by NIH/NCI grants R01CA214515, R01CA181081, and NSF GRFP Grant 1650042. The content is solely the responsibility of the authors and does not necessarily represent the official views of the National Cancer Institute or the National Institutes of Health. The authors have no relevant conflicts of interest to disclose.

References

Becker AE, Andrew HM, Schwoebel PR and Boone JM 2020 Cone beam CT multisource configurations: evaluating image quality, scatter, and dose using experimental study and Monte Carlo simulation Phys. Med. Bio in press. (10.1088/1361-6560/abc306)

Behling R 2018 X-ray tubes development – IOMP history of medical physics Med. Phys. Int 1 8–55

Boone JM, Becker AE, Hernandez AM, Dobbins JT and Schwoebel P 2019 Multi-x-ray source array for stationary tomosynthesis or multi-cone angle cone beam CT Proc. SPIE 10948

Boyd DP, Couch JL, Napel SA, Parker DL, Peschmann KR, Rand RE and Herrmannsfeldt WB 1982 High-speed, multi-slice, x-ray computed tomography Proc. SPIE 0372

Bushberg JT, Siebert JA, Leidholdt EM and Boone JM 2012 The Essential Physics of Medical Imaging (Philadelphia, PA: Lippincott, Williams, and Wilkins)

Calliste J, Wu G, Laganis PE, Spronk D, Jafari H, Olson K, Gao B, Lee YZ, Zhou O and Lu J 2017 Second generation stationary digital breast tomosynthesis system with faster scan time and wider angular span Med. Phys 44 4482–95 [PubMed: 28569999]

Godfrey DJ, Mcadams HP and Dobbins JT III 2013 The effect of averaging adjacent planes for artifact reduction in matrix inversion tomosynthesis (MITS) Med. Phys 40 021907 [PubMed: 23387755]

Godfrey DJ, Rader A and Dobbins JT III 2003 Practical strategies for the clinical implementation of matrix inversion tomosynthesis (MITS) Proc. SPIE 5030 379–390

Horvat JV, Keating DM, Rodrigues-Duarte H, Morris EA and Mango VL 2019 Calcifications in digital breast tomosynthesis: imaging features and biopsy techniques RadioGraphics 39 307–18 [PubMed: 30681901]

Kandlakunta P, Pham R, Khan R and Zhang T 2017 Development of multi-pixel x-ray source using oxide-coated cathode Phys. Med. Biol 62 N320–N336 [PubMed: 28145276]

Kleint C 1993 On the early history of field emission including attempts of tunneling spectroscopy Prog. Surf. Sci 42 101–15

Kohl WH 1967 Handbook of Materials and Techniques for Vacuum Devices (New York: Reinhold Publishing Corporation)

Kopans DB 2014 Digital breast tomosynthesis from concept to clinical care Am. J. Roentgenol 202 299–308 [PubMed: 24450669]

Mertelmeier T 2014 Filtered backprojection-based methods for tomosynthesis image reconstruction Tomosynthesis Imaging eds Reiser I and Glick SJ (Boca Raton: Taylor & Francis) p 101

For example see:(a)Morgan H Rotating anode X-ray tube with multiple simultaneously emitting focal spots U.S. Patent 6,125,167 (26 9. 2000),(b)Mistretta C, Patch S, Boutchko R, Hsieh J, ‘Computed

tomography with *z*-axis scanning' U.S. Patent 20050100126 (12 5 2005),(c)Dafni E, 'X-ray tube' U.S. Patent 8,693,638

Neculaes VB et al. 2016 Multisource inverse-geometry CT. Part II. X-ray source design and prototype Med. Phys 43 4617–27 [PubMed: 27487878]

Neculaes VB, Edic PM, Frontera M, Caiafa A, Wang G and De Man B 2014 Multisource x-ray and CT: lessons learned and future outlook IEEE Access 2 1568–85

Oosterkamp WJ 1948 The heat dissipation in the anode of an x-ray tube Philips Res. 3 pp 161–73 Part 1 pp 49–59, Part 2 Part 3 pp 303–317

Reference Data for Radio Engineers 1981 Electron Tubes ch 17 (Howard Sams and Co/ITT: New York) p 17–8

Sechopoulos I. 2013; A review of breast tomosynthesis. Part I. The image acquisition process. Med. Phys. 40 :014301. [PubMed: 23298126]

Shrestha S, Vedantham S and Karellas A 2017 Towards standardization of x-ray beam filters in digital mammography and digital breast tomosynthesis: Monte Carlo simulations and analytical modelling Phys. Med. Biol 62 1969–1993 [PubMed: 28075335]

Siemens. SOMATOM Dual Source CT Scanners. 2020. https://www.siemens-healthineers.com/en-us/computed-tomography/dual-source-ct

Smith, A; Design considerations in optimizing a breast tomosynthesis system. 2013. http://hologiced.com/assets/Design_Considerations_Optimizing_Breast_Tomo.pdf

Tirada N, Li G, Dreizin D, Robinson L, Khorjekar G, Dromi S and Ernst T 2019 Digital breast tomosynthesis: physics, artifacts, and quality control considerations RadioGraphics 39 313–426

Zhu W (ed) 2001 Vacuum Microelectronics (New York: John Wiley and Sons)

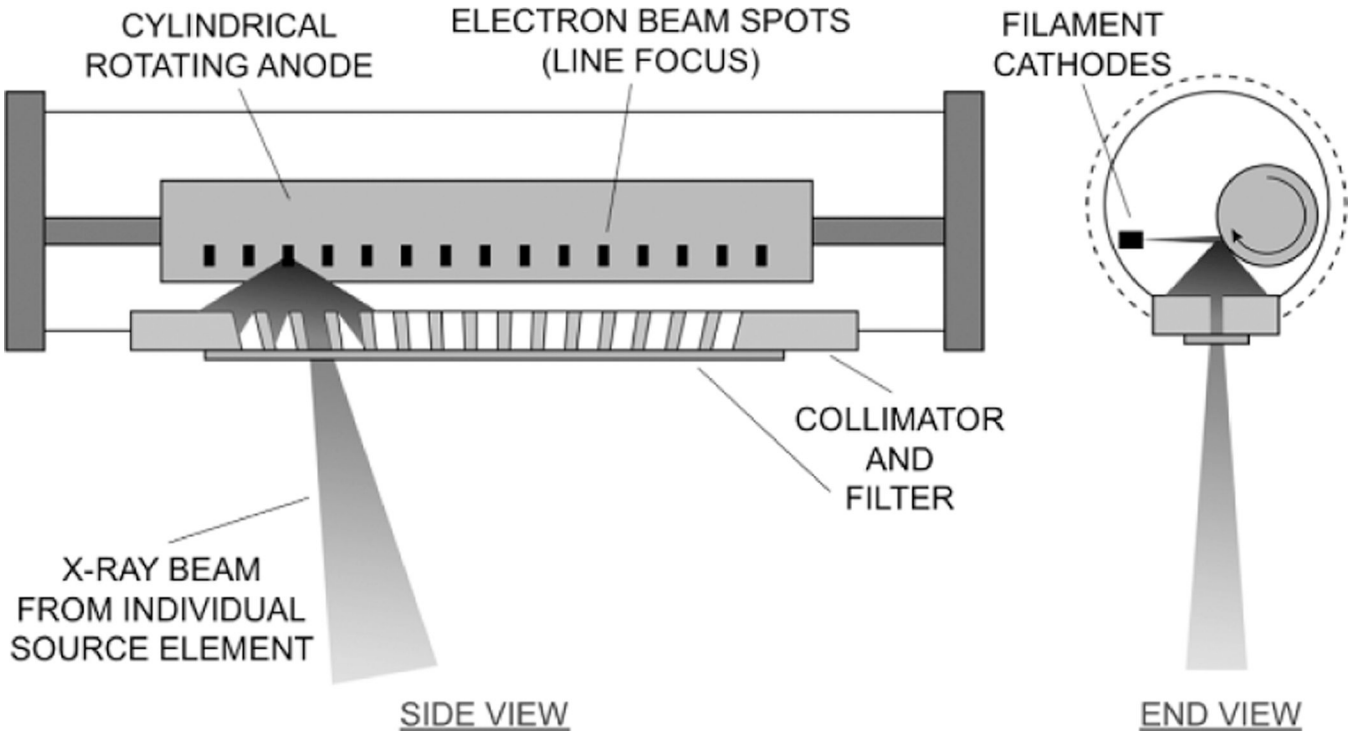

Figure 1.
Schematic of the MXA source with rotating anode assembly as applied to digital breast tomosynthesis.

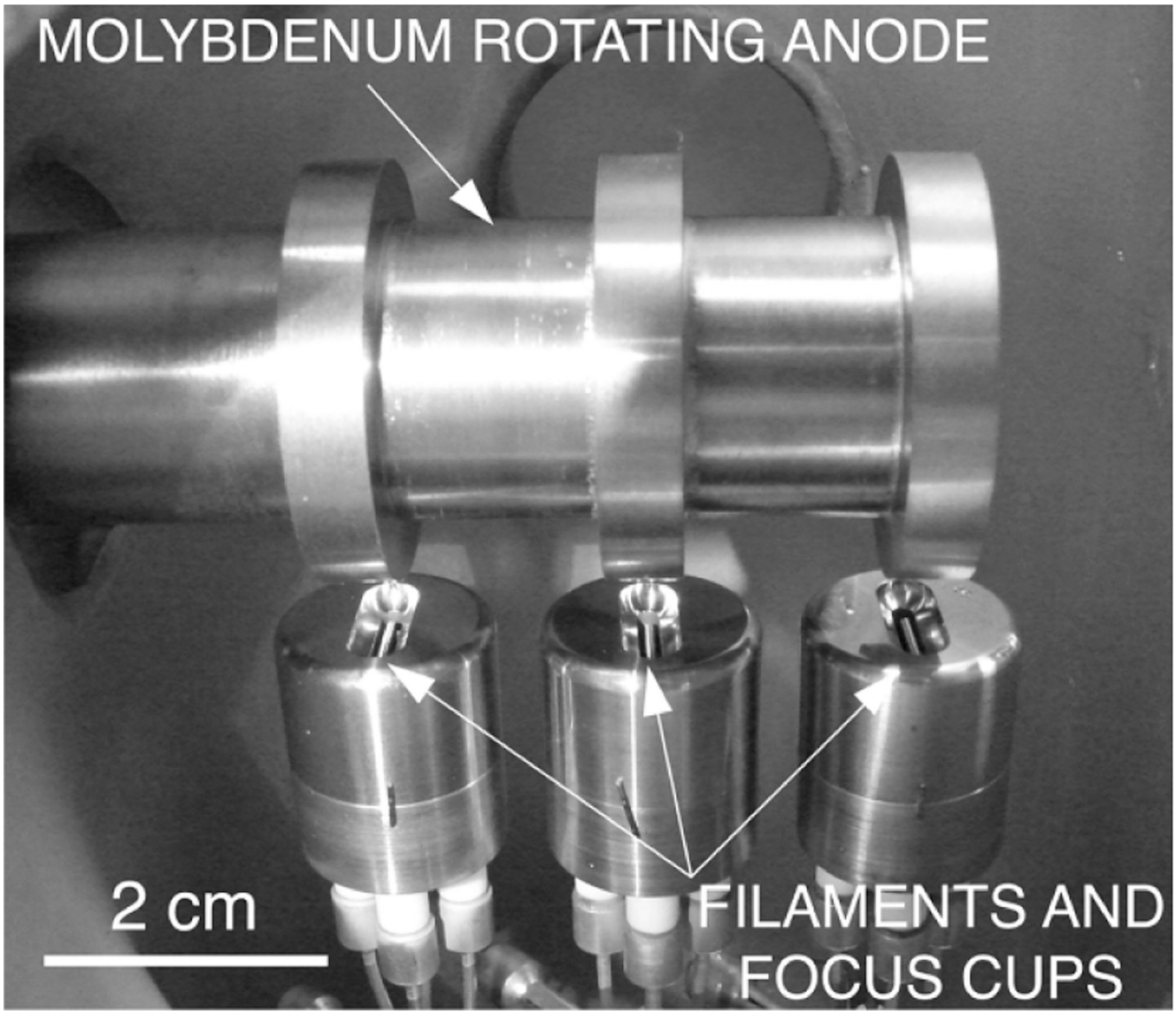

Figure 2.
Photograph of the 3-source element MXA showing the solid molybdenum rotating anode and grid-controlled tungsten filament cathodes.

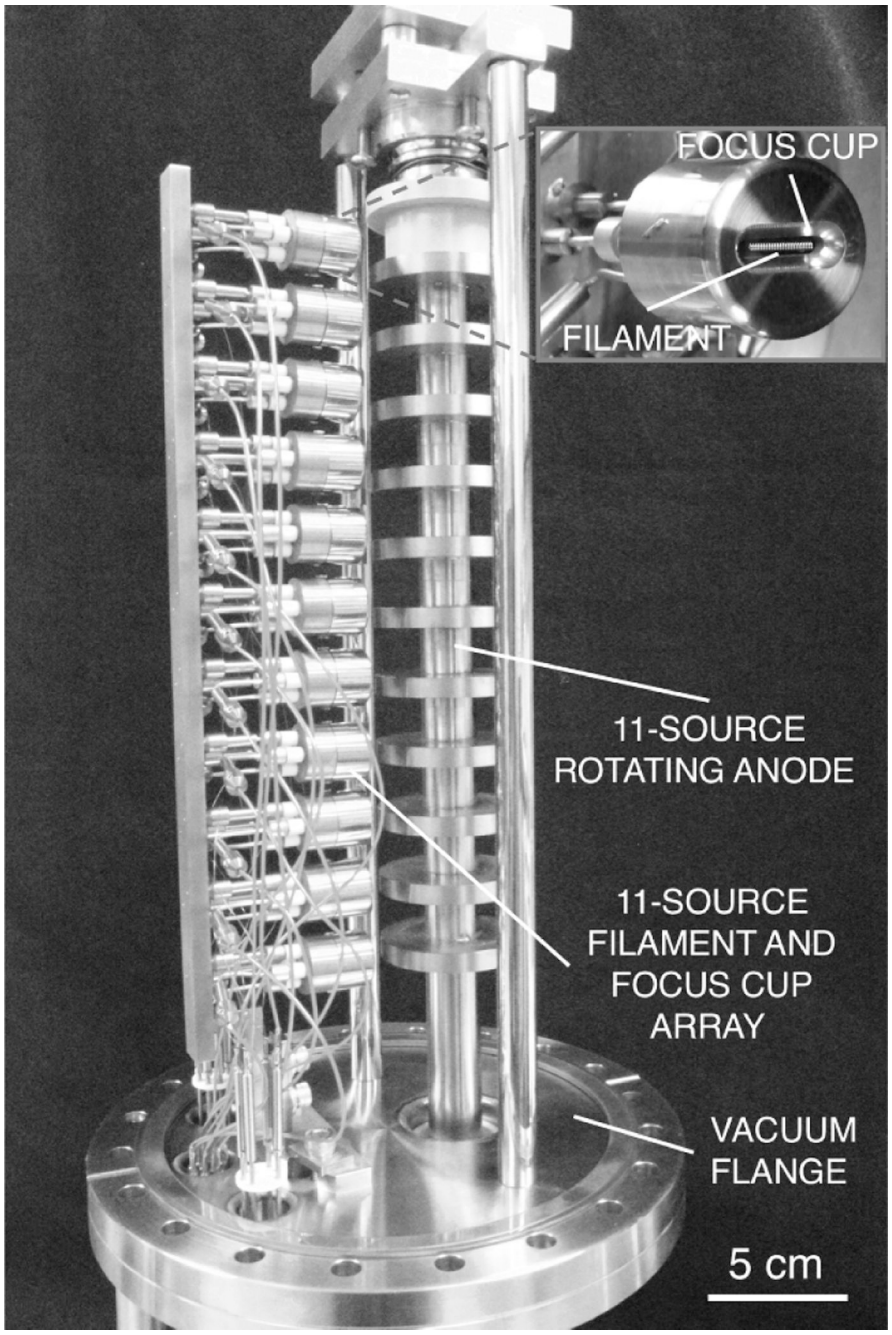

Figure 3.
Photograph of the 11-source element DBT MXA with a close-up of the filament and focus-cup-grid assembly of one source element.

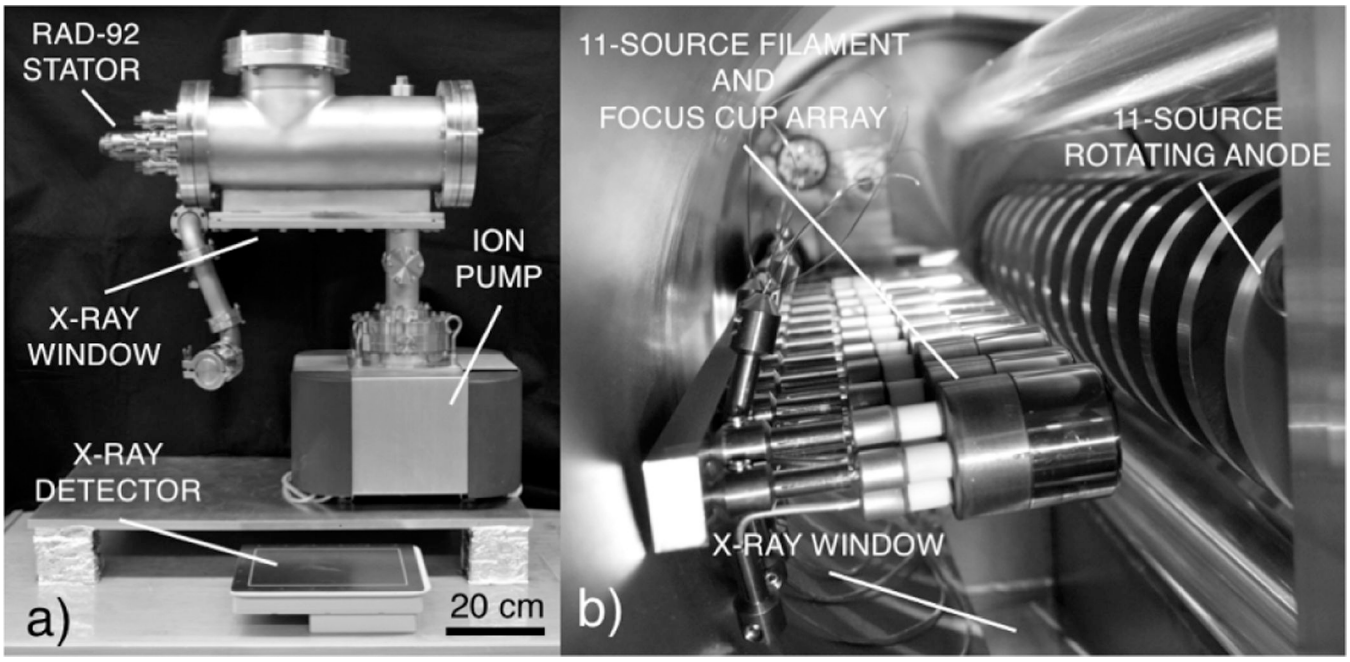

Figure 4.

Photographs of a) The prototype DBT system used for the 3-source element and 11-source element MXA, and b) the 11-source element MXA installed in the prototype DBT system.

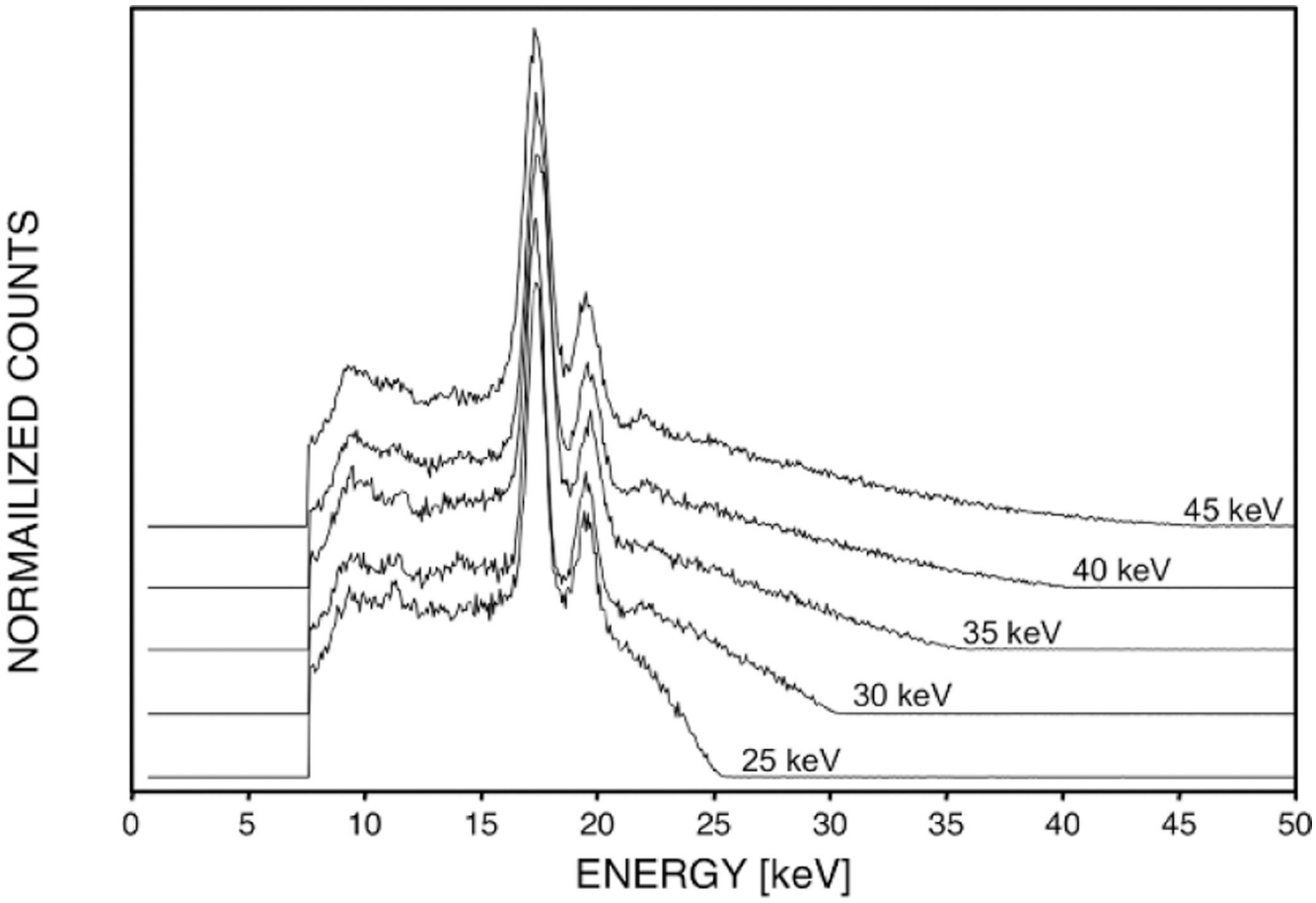

Figure 5.
X-ray spectra produced by a typical source element operating at electron energies from 25 keV to 45 keV in 5 keV increments.

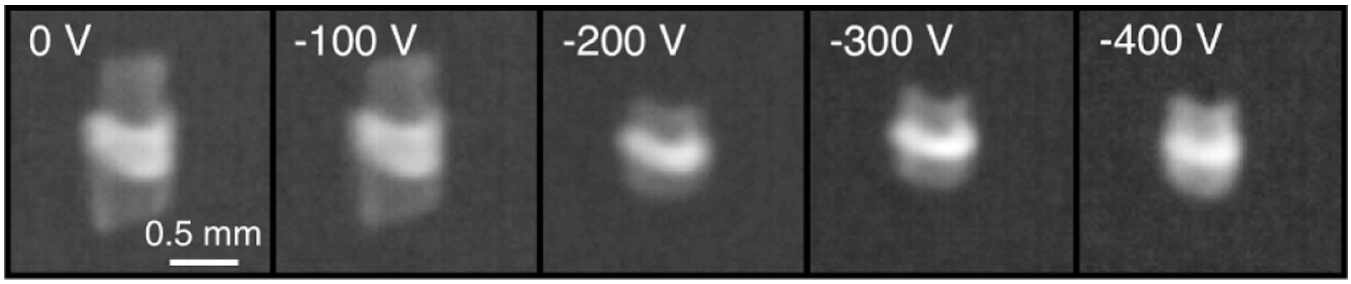

Figure 6.
X-ray pinhole camera images of the x-ray focal spot as the grid bias (focus cup bias) is changed. 45 kV, 50 mA.

Figure 7.

X-ray star pattern of a typical individual source element. Spot size is 0.3 mm × 0.3 mm for V_{grid} = −300 V at 45 kV and 50 mA. Magnification on detector = 1.8×.

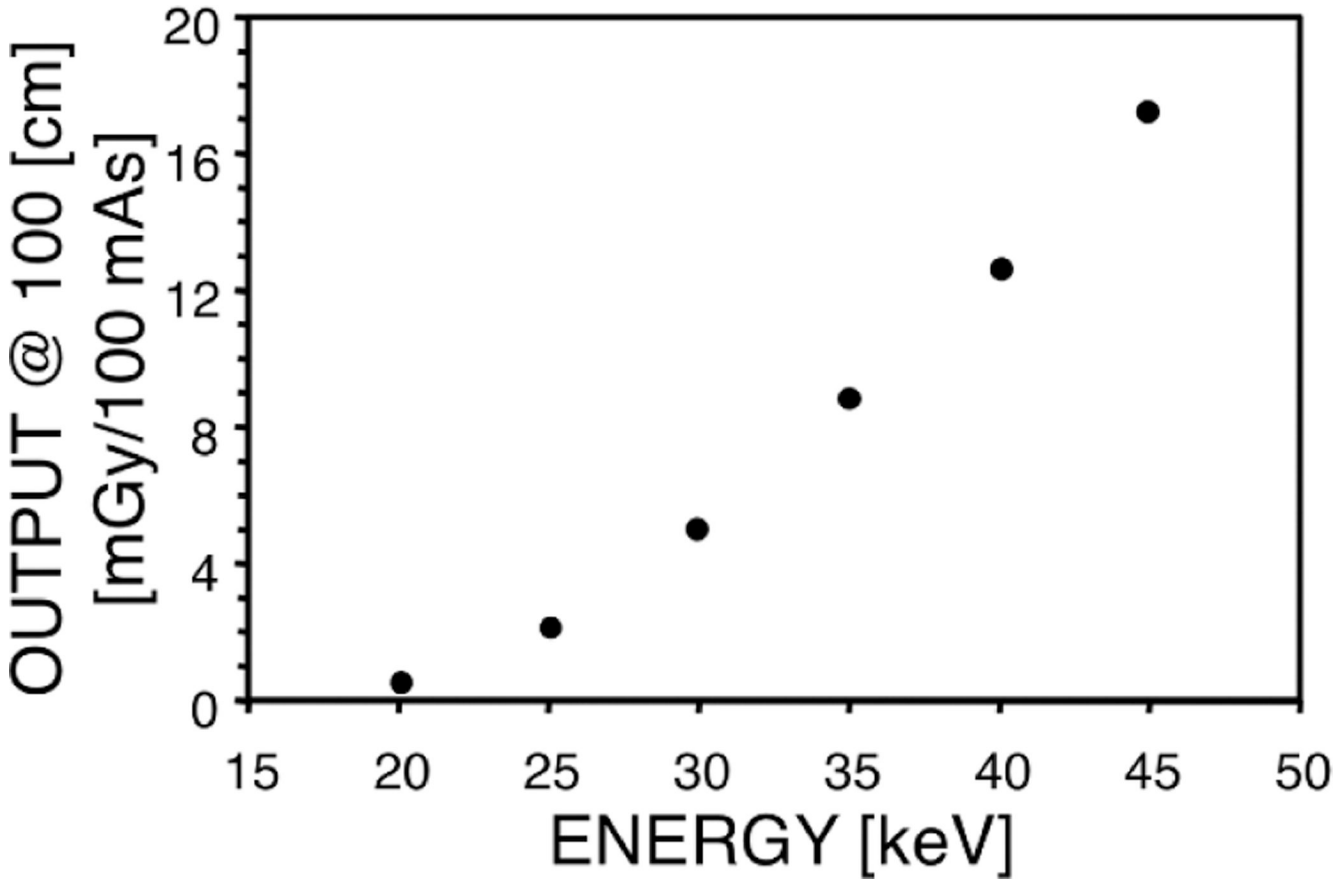

Figure 8.
Tube output from a typical element of the 11-source element MXA as a function of beam energy.

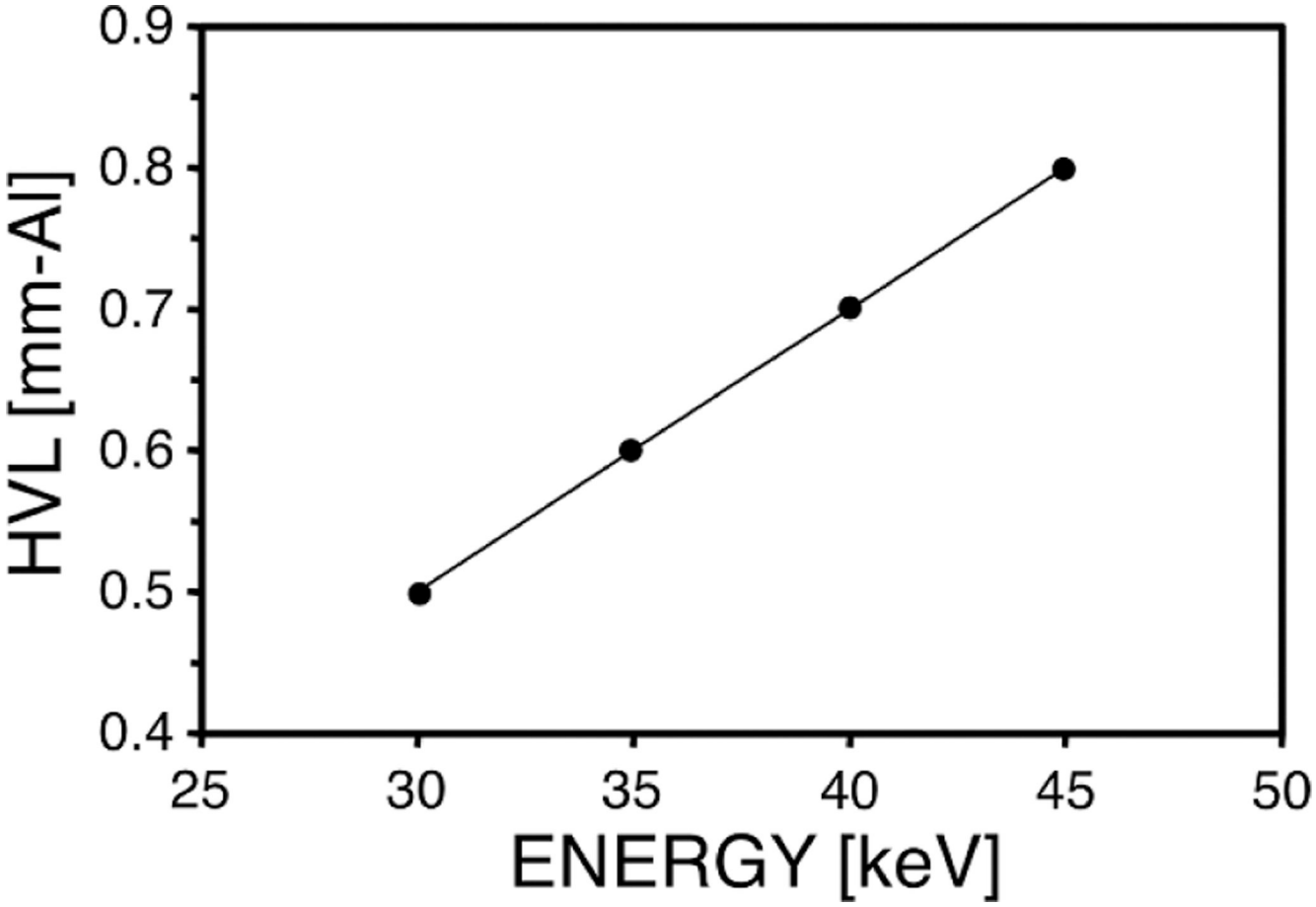

Figure 9.
Half-value layer measured with the 11-source element MXA at 50 mA.

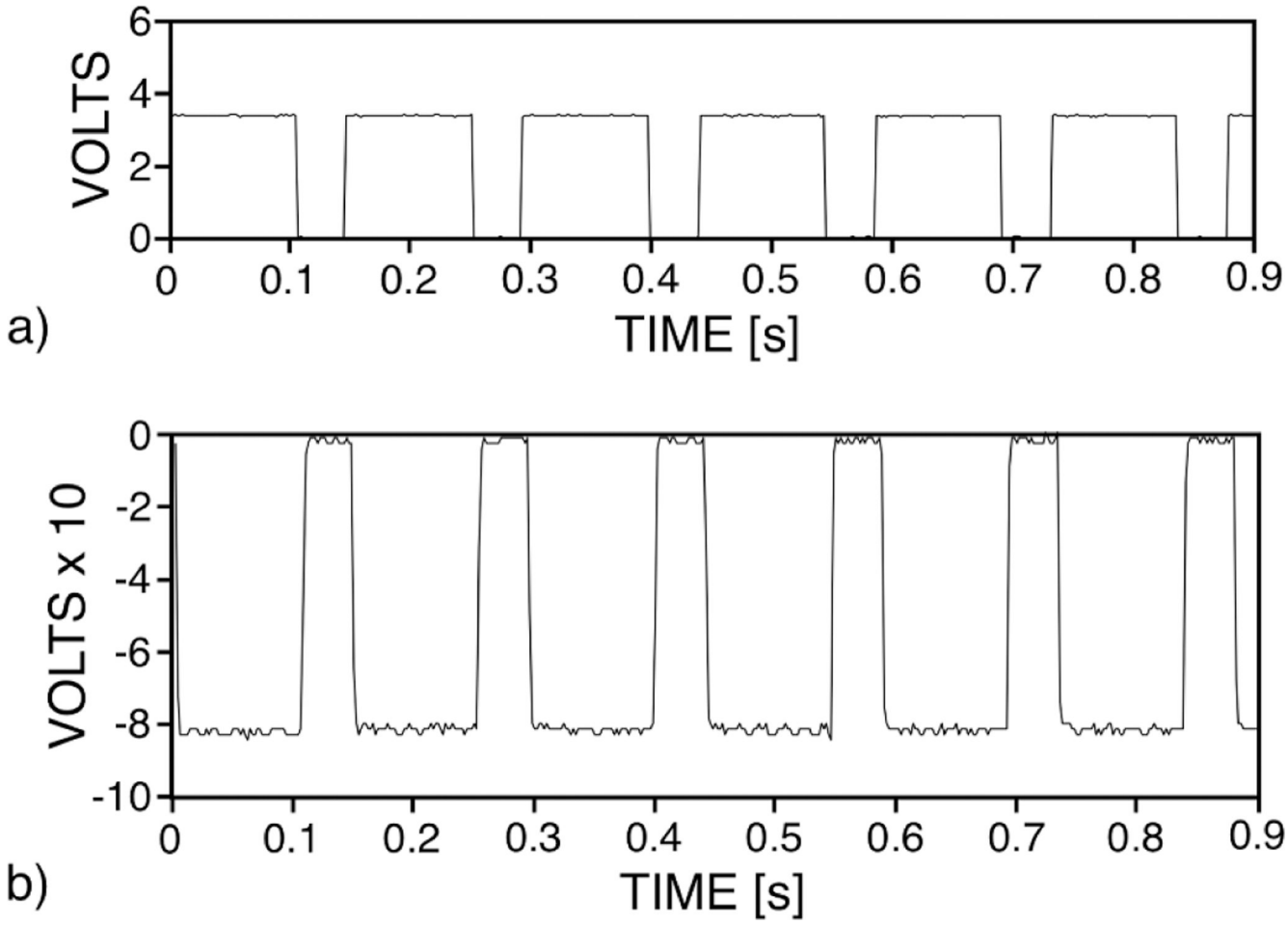

Figure 10.

Oscilloscope voltage versus time plots of the 3-element source cycling through each source element in sequence. a) The TTL logic pulse used to control the grid voltage. TTL high turns on the source; b) the signal from the x-ray detector showing a 110 ms duration x-ray pulse at a frequency of 7 Hz. The ON signal is at −0.8 V and the OFF signal is at 0 V.

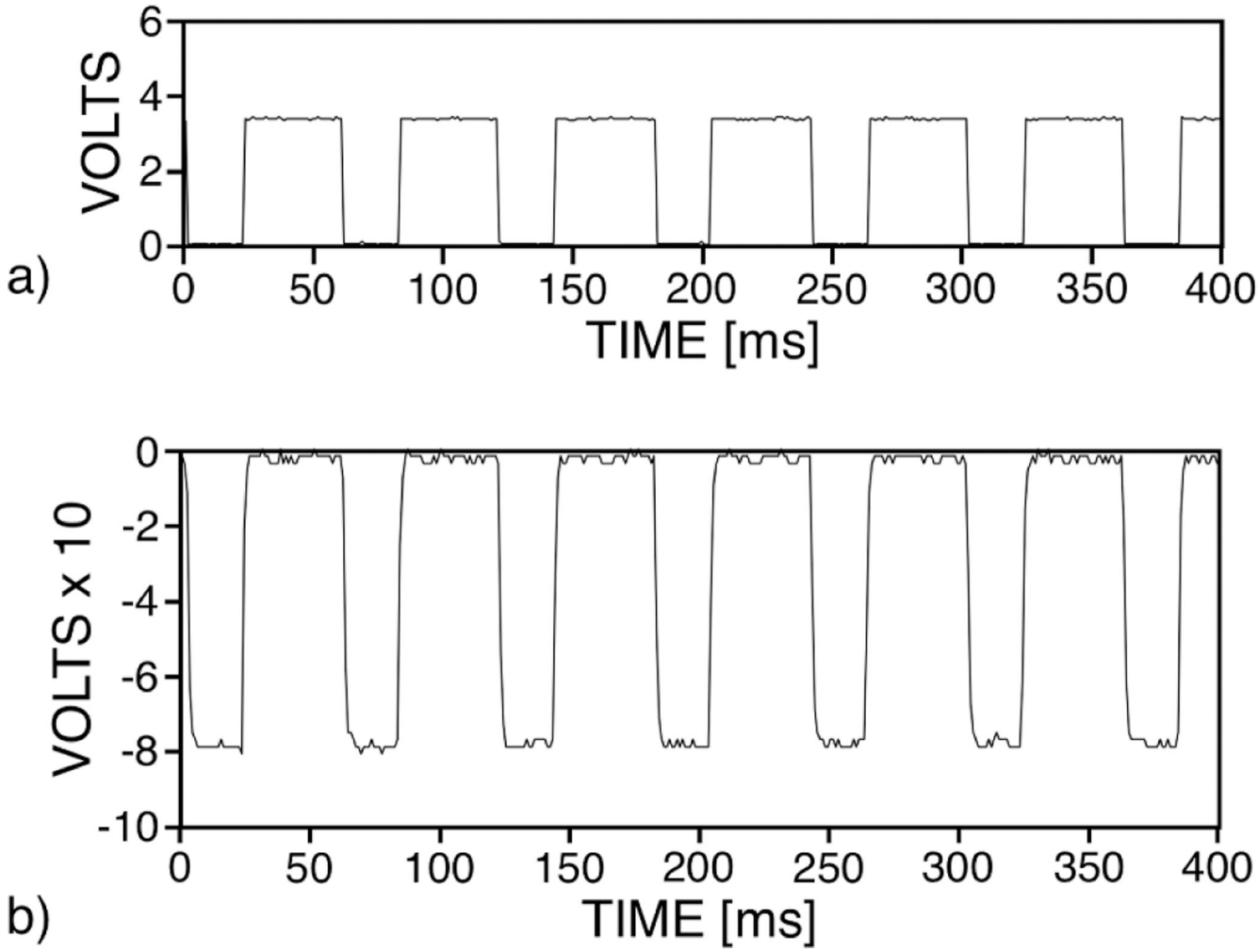

Figure 11.

Oscilloscope voltage versus time plots of the 3-element source cycling through each source element in sequence. a) the TTL logic pulse used to control the focus cup grid voltage; b) the signal from the x-ray detector showing a 20 ms duration x-ray pulse at a frequency of 17 Hz. The ON signal is at −0.8 V and the OFF signal is at 0 V.

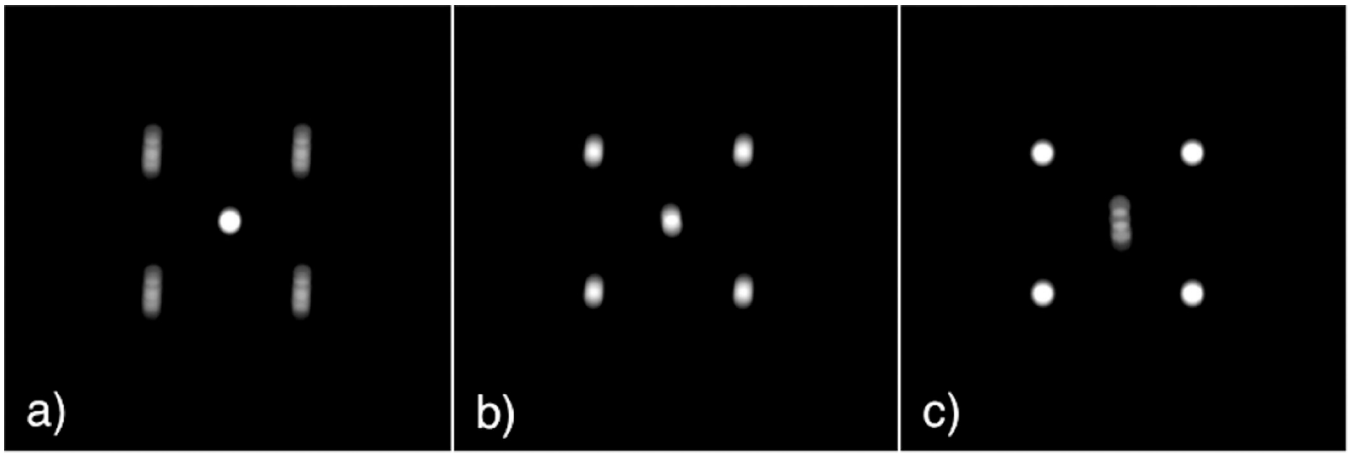

Figure 12.

Tomosynthesis images of the BB-phantom at three depths showing planes separated by 4.0 mm. The single BB at the apex of the right regular pyramid is furthest from the detector.

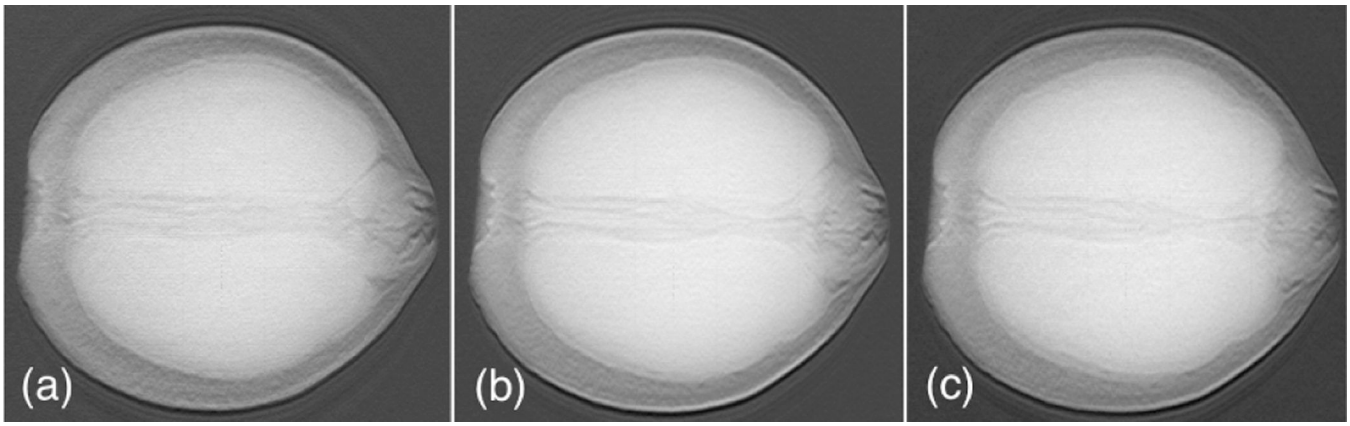

Figure 13.

Tomosynthesis images of an orange at three depths showing planes separated by 4.0 mm through the central core centered on the plane shown in (b).